A Measurement of the Extragalactic Background Light

Dennis Houlihan

*This work was submitted as part of a course requirement for completion of the BS degree in the Physics Program at RIT and, in its current form, does not appear in any publication external to RIT.**

(Dated: November 30, 2020)

The extragalactic background light (EBL) is the total light emitted from sources outside of the Milky Way Galaxy. An accurate measurement of the EBL can be used as a benchmark test to see if there are any extra components other than the light from galaxies. Any discrepancies would imply the presence of new diffuse emission sources and lead to discoveries such as diffuse photons associated with dark matter annihilation. In this project, we use data from the Linear Etalon Imaging Spectral Array (LEISA) aboard the New Horizons spacecraft to measure the EBL in the near-infrared range. We first perform preliminary data assessments and cuts to the publicly available LEISA data. We then compute the J2000 coordinates using rotation quaternions. Missing quaternion data from the FITS extension was substituted with quaternion data from the header, leading to inaccurate astrometry except for the middle frame of each image. Using the middle frame, we search for stars to mask so that their light contribution can be ignored in our measurement.

Introduction

The universe is home to a range of diffuse astrophysical backgrounds that, if measured accurately, can yield important insights into the process of cosmic structure formation. One such background, and the background of interest in this project, is the extragalactic background light (EBL). The EBL is the total emission of all light outside of our Milky Way Galaxy at all wavelengths[1]. Specific wavelength ranges in the EBL are remnants of specific emission sources. One component of this background is the Cosmic Microwave Background (CMB), which was emitted shortly after the Big Bang and is a prime example of how fruitful diffuse background studies can be as it is a major source of information about the early universe[2].

The infrared component of the EBL is referred to as the Cosmic Infrared Background (CIB). It is believed that the CIB is dominated by redshifted starlight[3]. Just as the CMB provides information on the early universe, measuring the CIB could potentially provide new information on stellar and galactic processes as well as reveal other sources of emission[4]. More specifically, a precise measurement of the EBL can be used as a valuable test where integrated light from discrete sources such as galaxies can be compared[2]. From this, constraints on models of galaxy formation and evolution[1], star formation, and metal and dust production[5] can be determined. Other potential results include discoveries such as diffuse photons associated with dark matter annihilation, the signature of recombination from the epoch of reionization, and the presence of intra-halo light in the intragalactic medium[4].

Prior ground-based measurement of the CIB has proven to be extremely difficult as there are numerous diffuse foregrounds that must be taken into account, as well as atmospheric extinction (absorption), scattering, and airglow emission[6]. The three most prominent foregrounds are the integrated star light (ISL), zodiacal light (ZL), and the diffuse galactic light (DGL)[4]. Foreground contribution is illustrated in Equation 1[2], which governs the brightness in an arbitrary image of the astronomical sky outside of Earth's atmosphere.

$$\lambda I_\lambda^{\text{meas}} = \lambda I_\lambda^{\text{IPD}} + \lambda I_\lambda^{*} + \lambda I_\lambda^{\text{RS}} + \lambda I_\lambda^{\text{DGL}} + \epsilon I_\lambda^{\text{EBL}} + \lambda I_\lambda^{\text{inst}} \quad (1)$$

Where $\lambda I_\lambda^{\text{IPD}}$ is the brightness associated with the IPD (ZL), λI_λ^{*} is brightness from resolved stars, $\lambda I_\lambda^{\text{RS}}$ refers to brightness from residual starlight of stars too faint to detect individually, $\lambda I_\lambda^{\text{DGL}}$ refers to the brightness from the DGL, ϵ is a factor that accounts for absorption in galactic dust, and $\lambda I_\lambda^{\text{inst}}$ refers to the instrument noise. We can isolate $\lambda I_\lambda^{\text{EBL}}$ in three steps[7]: remove the effect of λI_λ^{*} by masking bright stars; subtract the diffuse components to isolate the diffuse residual component $\lambda I_\lambda^{\text{resid}} = \epsilon I_\lambda^{\text{EBL}}$; and correct the mean residual intensity for the effects of galactic extinction (determine value of ϵ) to yield $\lambda I_\lambda^{\text{EBL}}$.

The ISL is the total sum of light emitted from stars within the Milky Way Galaxy[8] and corresponds to both λI_λ^{*} and $\lambda I_\lambda^{\text{RS}}$. It is easy to account for brighter stars, however, there are faint stars that are below the detection threshold of a given image that still contribute to this foreground. Taking advantage of real observations and star population models such as the TRILEGAL model[2] will be needed to estimate the faint stars contribution.

The ZL is caused by solar light scattered by interplanetary dust particles within the plane of the ecliptic[2]. This dust originates from many sources such as comets, asteroids, and Edgeworth-Kuiper Belt objects and disperse after they are ejected from their parent bodies[2]. The ZL is concentrated within the plane of the ecliptic and is less appreciable outside of it[8]. Furthermore, IPD in general is more prominent within the inner solar system, as measurements from Helios, Galileo, and Pioneers 8/9 show a steep decline in IPD density outside of 1AU[4] and confinement to within 30° of the ecliptic plane.

In a similar way to the IPD, dust along the plane of the Milky Way scatters light from stars within the galaxy. The resulting foreground is known as the DGL ($\lambda I_\lambda^{\text{DGL}}$). As the ZL is brightest along the ecliptic, the

DGL is brightest in the galactic plane and fainter at higher galactic latitudes[7]. It is important to note that the DGL is due to dust in interstellar space, not interplanetary space. Therefore, outer-solar system location does not mitigate this light contribution and no where in the sky can we ignore this foreground.

One way around the brightest of these foregrounds is the use of instruments aboard New Horizons[9], a NASA spacecraft sent to survey Pluto, its moons, and other objects in the outer solar system. In addition to their original purpose, New Horizons instruments can be used for astronomical measurements. This provides a rare and exciting opportunity to measure the EBL as a whole from an outer solar system vantage point that is free from the Earth's atmosphere and substantially decreases the effect of the ZL. The goal of this capstone project is to make a good measurement of the CIB in the near infrared spectral range with data from the New Horizons instrument known as the Linear Etalon Imaging Spectral Array (LEISA)[9].

The first phase of this project focused mainly on learning about LEISA's instrumentation and data pipeline, performing preliminary data assessment and cuts, as well as finding where the image is pointing in order to find stars. These are important preparatory steps because in order to make accurate measurements of the CIB, we need to understand how LEISA's parameters affect the data and if the data we use is optimal for our purposes. Knowing where the images are pointed is also extremely important because the light contribution of stars is needed to be taken into account.

The LEISA Instrument

Launched on January 19, 2006, the New Horizons spacecraft was NASA's first mission to explore Pluto and its moons Charon, Nix, and Hydra[9]. It is currently in an extended mission focused on Kuiper Belt science at heliocentric distances of beyond 50AU[4] and will continue on this mission until at least 2021.

While the main purpose of New Horizons and its instruments is to map the surface geology and composition of these objects[9], its instruments can double as astronomical telescopes with which EBL measurements can be made. One of the core instruments aboard the New Horizons spacecraft is *Ralph*[9], a visible/near-IR multispectral imager. It consists of a telescope that feeds two sets of focal planes that are intended to provide color, composition, and thermal maps for the surfaces of Pluto and its moons[9]. At one of these focal planes is the Multi-Spectral Visible Imaging Camera (MVIC) and LEISA[10].

LEISA is a wedged filter infra-red spectral imager and the instrument of choice for this project. The detector is a 256×256 pixel array whose filter is separated into two pieces: a high and low spectral resolution segment bonded together. The wavelength range of the sensor is 1.225-2.5μm for the low resolution segment and 2.1-2.25μm for the high resolution segment[11]. The wavelength of the filter varies along each row, meaning each row measures a specific wavelength. The number of spectral channels is the number of rows excluding four rows[11] blocked by the adhesive connecting the two segments.

LEISA Instrument Parameters	
FOV:	$0.9^\circ \times 0.9^\circ$
Single Pixel FOV:	12.38 arcsec × 12.38 arcsec
Pixel Size:	40μm × 40μm Pixels
Telescope Aperture:	75mm
Telescope Focal Length:	657.5mm
Spectral Resolution:	$\lambda/\Delta\lambda = 240$
Dark Current:	40 counts/second
Per-pixel Sensitivity:	6×10^4nWm^{-2}sr^{-1}
Expected CIB Signal:	10 nWm^{-2}sr^{-1}
In Track FWHM:	1.40±0.13 Pixels

TABLE I: Tabulated parameters for LEISA. All values were found in the Ralph instrument paper[10].

Compared to MVIC and LORRI, LEISA has a much higher wavelength range (1.25 - 2.5μm), which helps in detecting near-IR sources such as redshifted starlight in galaxies. LEISA also has a large field of view (0.9° x 0.9°)[10], which is good since the EBL is spread throughout the sky. Having a large field of view means measuring a larger area in the sky, which will help get a better sense of the nature of the EBL. LEISA's wavelength range is also important as measurements from 1-3μm have been very challenging on Earth[5] due to the bright foregrounds mentioned.

Although its vantage point avoids the bright ZL, LEISA's parameters are not optimal for measuring the EBL. In Table I, LEISA's parameters are listed. For example, LEISA's small aperture (75mm) and spectral resolution (R = 240) means that it has a poor per-pixel sensitivity[4]. This in turn requires a significantly longer integration time (∼1 day as compared to ∼1 hour for MVIC and LORRI)[4] to make a constraining measurement of the CIB. This coupled with the short integration times of the images from the publicly available datasets[12,13] made it almost impossible to detect stars with magnitudes ranging from 6-10. This issue is outlined in more detail in the later sections.

LEISA Data Structure and Pipeline

The LEISA detector array is a Rockwell PICNIC device[14] in Correlated Double Sample (CDS) mode[11]. The CDS technique consists of sampling a voltage output in two specific instants, the first one in a known condition and the second one in an unknown condition. This leads to a differential read out and removes the unwanted offset[15]. The signal is then converted in a 12-bit value using the middle of a 16-bit analog to digital (A/D) con-

verter. There are two data transfer modes: subtracted and un-subtracted modes[11]. Subtracted mode is when the reset level data is subtracted from the signal level data and the difference is returned. Un-subtracted mode is when signal and reset level are both returned.

The LEISA data is recorded in the form of data cubes[11], which are a collection of N number of exposures or frames, where N is determined by multiplying the length of the scan by the frame rate. The frame rate varies from 0.25 to 8 Hz, corresponding to a maximum exposure time of 4s and a minimum of 0.125s. LEISA often operates in scanning mode[11], where a target(s) is scanned across the filter, row by row. Using this method, an IR spectrum of a target or area can be achieved.

Data recorded on New Horizons is sent to Earth via the Deep Space Network. The data is then sent to the Mission Operations Center (MOC) at the Applied Physics Laboratory (APL)[11]. From there, the data is sent to the Science Operations Center (SOC) who converts the data from the MOC archives into Flexible Image Transport (FITS) files with calibrated data[11].

Raw Data Processing

The data cubes are stored in Band Interleaved by Line (BIL) order. BIL stores pixel information band by band for each line, or row, of the image[16]. In other words, each frame is stored sequentially. There are three steps taken to re-order the data received from the spacecraft[11]: de-interlace by quadrant; reverse the Y direction; rotate 180 degrees. The resulting data is packaged once again into a FITS file with the data cube stored as the primary data unit[11].

Calibration Pipeline

There are six steps applied to the raw LEISA data to produce the calibrated output[11]: (1) validate the raw image file; (2) preprocess un-subtracted mode data; (3) process A/D rollover pixels; (4) convert raw counts to calibrated values; (5) compute pointing data; (6) construct FITS file.

To validate the raw image file, checks are made for valid mode, instrument, mission, and image array size. The values of keywords are also validated in this step. In step (2), the reset values are subtracted from any data that was in un-subtracted mode. Step (3) corrects for A/D rollover pixels. If a file exists that identifies rollover pixels, then those pixels are corrected. If not, then any subtracted count that is greater than 3850 is considered to be rolled over and 4096 is subtracted from the raw count value[11].

Step (4) uses eight values to convert the raw signal count to a calibrated signal value[11]: electronics induced readout signal; CCD flat field; calibration offset; calibration gain; integration time; filter width; pixel solid angle; and gain correction. The induced readout signal is a base signal that is derived from studies of dark frames and is subtracted from the raw counts. The CCD flat field, calibration offset, and calibration gain are derived from lab data and refined by in-flight data. As the mission progresses, these values change, so different flat fields and calibration values can be used for an individual or group of observations[11]. These values, along with the integration time, filter width, pixel solid angle, and gain correction are all divided into the calibrated counts[11].

The pointing data of each pixel is computed in step (5) using the timing information from observations, ephemeris and attitude files, as well as the known optical distortion of LEISA. An array containing the cartesian pointing vectors of each pixel in the instrument reference frame are generated. Another array generated consists of the rotation quaternion of the instrument boresight into the J2000 reference frame for the middle of each frame. Finally, in step (6), a FITS file is constructed to store all image and processing data.

Preliminary Data Cuts

Before we could start our analysis, data assessment and cuts were performed to ensure the images we study are optimal for our purposes. Factors such as exposure time, type of image, and the presence of bright objects were all considered when determining whether to validate an image. The first thing I did was write a Python code that looped through the LEISA data sets and printed the values for exposure time as well as other header keywords that provide descriptions of the image.

Once I had a list of these keywords, I immediately cut images with exposure times less than four seconds from consideration. We need images with longer exposure times because LEISA's sensitivity is very poor and the EBL is very faint and four seconds is the maximum exposure time in any LEISA image. I then checked each image for any defects or bright objects that may hinder our ability to measure the faint EBL signal. Fortunately, each image with exposure time of four seconds did not have such defects. After completing the preliminary cuts, we were left with eight images that we deemed acceptable for our purposes: two images from the Pluto Encounter Phase and six images from the Pluto Cruise Phase of the New Horizons Mission[12].

Post-Reduction Analysis

The focus for this semester was to exclude the brightness from the resolved starlight, or λI_λ^* from Equation 1. To do this, we needed to implement image masks to remove signals from unwanted sources. Masking is the process of identifying and ignoring stars or other sources of light that are near or brighter than the detection threshold from an image[7]. One can identify stars

using various catalogues that are publicly available, such as the Gaia DR2 catalog[17]. Successfully implementing masks in our images ensures that we can effectively ignore bright contributions to the sky brightness from stars, hot pixels, and other defects in our images.

Before masking the stars, we first needed to compute the celestial coordinates for each pixel in the images. Then, we can compare the stars found in the image with the objects in the Gaia DR2 catalog. From there, we can mask the appropriate pixels in the image. This procedure was not completed due to complications arising from the instrument's quaternion data and LEISA's poor sensitivity preventing us to both locate and see the stars in the images.

Instrument Pointing

Calculating the instrument pointing is crucial for our goal of measuring the EBL. As stated before, accurate astrometric data allows us to locate and mask bright stars in the images. LEISA utilizes rotation quaternions to allow the user to calculate the J2000 cartesian pointing vectors of each pixel[11]. In extension 3 of each FITS file, the cartesian pointing vectors of each pixel in the instrument reference frame is stored as a 256×256×3 array. In extension 7 of each FITS file, the ephemeris time and quaternion for the center of each frame is stored as a 5×N array, where N is the number of frames in the image. By rotating the pointing vectors by the given quaternions, the cartesian J2000 vectors can be derived. From there, the Right Ascension and Declination coordinates of each pixel can be calculated by converting these vectors into polar coordinates.

Right Ascension and Declination are celestial coordinates that describe an object's position on the sky[18]. Just as cities need longitude and latitude coordinates, each object in the sky needs Right Ascension and Declination coordinates to fix its location. Because Right Ascension and Declination are constantly changing due to Earth's precession, these coordinates are referenced to a specific epoch. J2000 is presently the standard Julian epoch that is based on Julian years of exactly 365.25 days. J2000 refers to January 1, 2000, noon TT (Terrestrial Time)[18].

Quaternion Rotations

To understand how to rotate a vector with a quaternion, one must first understand what a quaternion is. A quaternion is a 4-element vector composing of one real and three complex elements. Unlike Euler angles that rotate vectors by a series of rotations around the X, Y, and Z axes, a quaternion rotates a vector about a rotational axis, that is not necessarily the X, Y, or Z axis[19]. First, let the standard cartesian basis $\mathbf{i}$, $\mathbf{j}$, $\mathbf{k}$ satisfy the following condition:

$$\mathbf{i}^2 = \mathbf{j}^2 = \mathbf{k}^2 = \mathbf{ijk} = -1 \tag{2}$$

We can then define a quaternion as the sum of a scalar and a vector:

$$\bar{q} = q_0 + \mathbf{i}q_1 + \mathbf{j}q_2 + \mathbf{k}q_3 = q_0 + q \tag{3}$$

where

$$q = \mathbf{i}q_1 + \mathbf{j}q_2 + \mathbf{k}q_3 \tag{4}$$

For LEISA, and for aerospace engineering in general[19], a special normalized quaternion $q_0 = \cos\frac{\alpha}{2}$ and $q = \hat{e}\sin\frac{\alpha}{2}$ is used, where α is the rotational angle and $\hat{e}$ is the rotation axis. Say we have a vector that we want to rotate $\bar{v}$:

$$\bar{v} = a\mathbf{i} + b\mathbf{j} + c\mathbf{k} \tag{5}$$

To perform this rotation, we have to take the tensor product between the vector, the quaternion, and the complex conjugate of the quaternion. It is important to note that quaternions are non-commutative[19], which means that the product of two quaternions depends one what quaternion is on the left and what is on the right. In other words, order matters. So if we define $\bar{w}$ as the resulting vector of $\bar{v}$ being rotated by the quaternion $\bar{q}$, then it should look like:

$$\bar{w} = \bar{q} \otimes \bar{v} \otimes \bar{q}^* \tag{6}$$

Where $\otimes$ denotes a tensor product. For LEISA, $\bar{q}$ would be the quaternion stored in extension 7 of the FITS file, $\bar{v}$ would be the cartesian pointing vector in the instrument fixed body frame, and $\bar{w}$ would correspond to the resulting cartesian J2000 pointing vector. The next step is to use the J2000 pointing vectors to calculate the Right Ascension (α or RA) and Declination (δ or Dec) coordinates of each pixel. As a note, I will be using RA and Dec in text but α and δ in equations for Right Ascension and Declination, respectfully. To calculate RA and Dec, we must convert our J2000 pointing vectors from cartesian to polar coordinates. If we think of the unit circle, RA would be the azimuthal angle while Dec would be the polar angle. Therefore, we can relate the J2000 cartesian coordinates (X,Y,Z) to the polar coordinates (α,δ):

$$X = \cos\alpha\cos\delta \tag{7}$$

$$Y = \sin\alpha\cos\delta \tag{8}$$

$$Z = \sin\delta \tag{9}$$

Solving for δ in Equation 9, we see that Dec can be expressed as:

$$\delta = \arcsin Z \tag{10}$$

By dividing Equation 8 by Equation 7, we can find an expression for RA:

$$\alpha = \arctan \frac{Y}{X} \tag{11}$$

I attempted to perform this procedure for each pixel in each frame of the LEISA images, but found the third imaginary, or z-component, of each quaternion was zero. Without a full quaternion, we were not able to calculate pointing data for every frame in the images.

Missing Quaternion Data

At first glance, having a zero z-component was nonsensical when comparing it to the quaternion given in the header, which corresponds to the middle frame of the image. The quaternions in the headers all had non-zero z-components. To make sure that this was a case of missing data, I performed several tests.

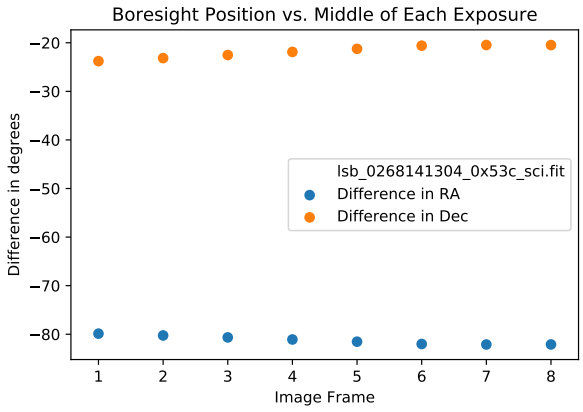

FIG. 1: Comparison of the boresight Right Ascension and Declination coordinates given in the header of the FITS files with calculated coordinates of the middle of each exposure using approach (1). The differences are substantial, implying the zero component of the extension quaternion is incorrect.

My tests were to rotate the vectors two different ways: (1) using the quaternions from the extension for each frame; (2) using the scalar and first two imaginary components of each quaternion from the extension with the z-component of the image header's quaternion. I then calculated the J2000 RA and Dec coordinates. Each header has a set of boresight RA and Dec coordinates that refer to the center of the middle frame. In each scenario, I compared the boresight coordinates that were given in the header with my computed J2000 RA and Dec coordinates of the middle of each exposure. Figure 1 shows the results of the approach (1). Considering the field of view of LEISA is $0.9^\circ \times 0.9^\circ$, these differences are considerable and prevent me from calculating accurate astrometric data with the given quaternions.

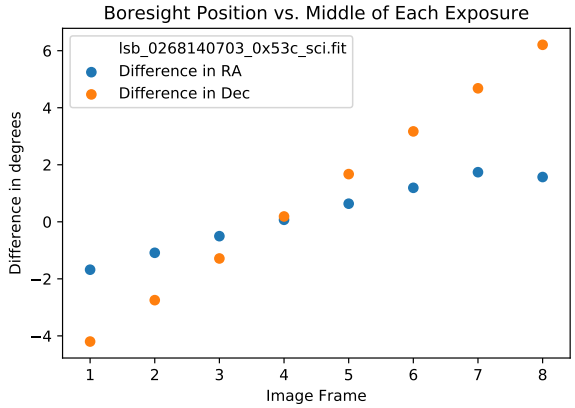

FIG. 2: Comparison of the boresight Right Ascension and Declination coordinates given in the header of the FITS files with calculated coordinates of the middle of each exposure using approach (2). One can see the differences are minimized in the middle exposure.

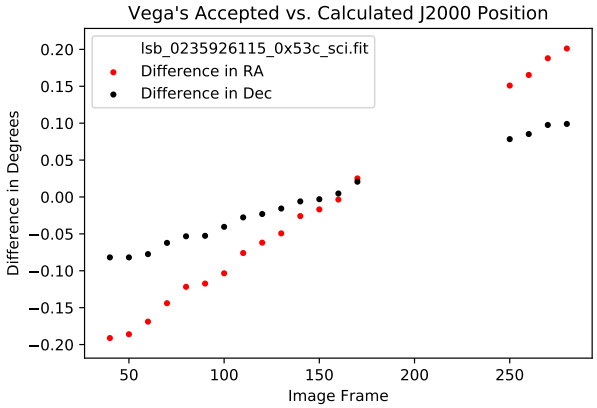

FIG. 3: Comparisons of Vega's position with the calculated position using approach (2). The differences in the accepted and calculated values are smallest in the middle frames and increase the farther away from the middle frames they are. This is expected as the quaternion from the header corresponds to the middle exposure of the image.

Figure 2 shows the results of using approach (2). This is a "band-aid" approach, which yields results that agree near the center frame, but get worse the further from the center exposure you go. I would expect this behavior if the third component of the quaternion information should be updated in each exposure; since the quaternion reported in the header is referenced to the middle integration, assuming that value should minimize the discrepancy. This clearly shows that information is missing, and the header value is not a complete description.

Another test I conducted was to track the star Vega in the image labeled lsb_0397097519_0x53c_sci.fit from the "Cruise to First KBO Encounter" data set[13].

This image was not validated for our purposes, we used this solely for this test. In this image, the star Vega is being scanned in a window as a slow scan test. For every ten frames, starting at frame 40, I recorded Vega's position on the image, and recorded my calculated RA and Dec coordinates for each using approach (2). Figure 3 above shows the difference between the calculated position of Vega for each frame (the missing data points are due to Vega passing through a very noisy section of the image, making it difficult to see where it was). Again, the differences are smaller towards the middle frames and get larger the farther from the middle frames you go. This is the same trend seen with the image boresight test.

A report about the missing quaternion data was made and sent to the manager of the Small Bodies Node of NASA's Planetary Data System, Dr. Ludmilla Kolokolova. We were told that the issue would be studied further and they will inform us as well as other LEISA users of the updates in the data set done to resolve the problem. However, no timetable was given for how long fixing the quaternion data would take.

The Search for Resolved Stars

While the missing quaternion data has significantly limited our ability to calculate accurate J2000 coordinates, there was still some work we were able to do. One thing was to find and mask any stars found in the middle frame. As shown before with image boresight and Vega test, the difference between the calculated and accepted values were minimized in the middle frames of the images. So ideally, we would be able to find stars in the middle frame at least.

Figure 4 shows an image from the Pluto Cruise data set. Simply looking at the image, no stars are apparent, which is true for our entire validated image set. The bright spots are due to instrument noise that is seen in each LEISA frame. However, I was able to see Vega in the prior test because Vega is a very bright star with an apparent V magnitude of about 0.026[20]. Fainter stars of magnitudes ranging from 6-10 are much harder to view due to LEISA's poor per pixel sensitivity. Because of this, programs such as Source-Extractor could not detect objects within the image. Source-Extractor simply searches an image for especially bright spots to identify objects and outputs various parameters such as flux, position, etc. for the identified objects[21]. With the stars very faint, and some noise very bright, we would run the risk of the program identifying noise as objects and ignoring the actual stars completely. Ultimately, we had to search for stars ourselves.

Instead of trying to find stars in the image and compare their coordinates to stars in a catalog, I decided to compare the positions of objects in the Gaia DR2 catalog[17] with each pixel in the middle frame of our images. I first created a query for objects within a box with length 0.9° (field of view of LEISA) centered

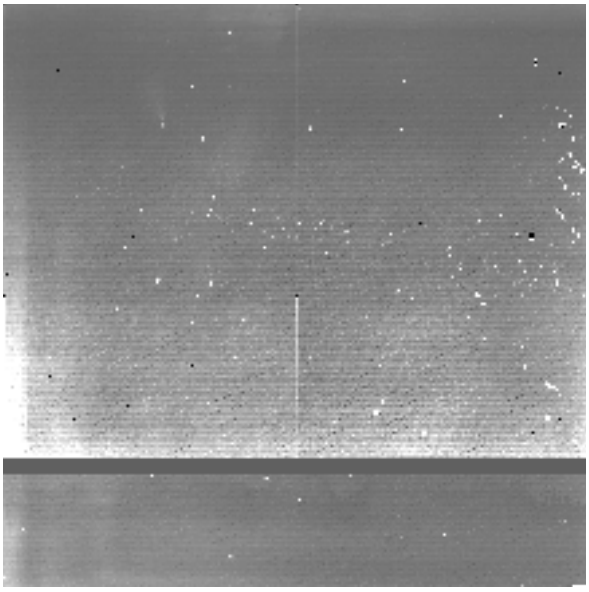

FIG. 4: The image lsb_0235926115_0x53c_sci.fit. The bright spots are instrument noise exhibited in every LEISA frame. There is also a considerable gradient exhibited in the low spectral resolution segment of the image.

at the boresight position listed in the header. I then ran a Python code that calculated the distance between the Gaia objects and each pixel in the image frame. It then paired each Gaia object with the closest pixel in the frame. Searching these pixels, I could not find any significant bright pixels that would usually indicate a star.

To help us see the stars, we attempted a few different techniques. One technique was to subtract the first frame of the data cube from the middle exposure in the hope that it would subtract the common noise/defects,

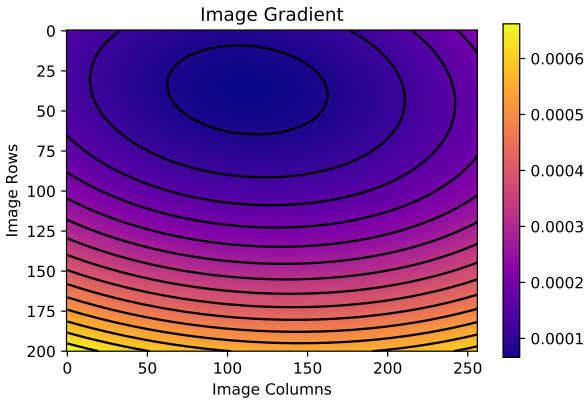

FIG. 5: Data fitted to a two dimensional parabola for the image lsb_0235926115_0x53c_sci.fit's low spectral resolution segment in the Pluto Cruise data set. The gradient is predominantly exhibited in the image's y-direction.

and hence make the stars more apparent. This did not make the stars any more noticeable, even after adjusting the scaling of the image frame. Next, we tried to sum all the frames in the data cube in the hopes that the stars would create a bright trail as the instrument moved across the field. Checks were made to make sure no especially bright or defective frames were included in the sum. Despite this, there were no trails exhibited in the image.

Finally, I attempted to correct the gradient that was exhibited in the low resolution segment of the images. To do this, I fit a two dimensional parabola to the image data. I then subtracted the fitted data from the original image. Figure 5 shows the fitted data for the image lsb_0235926115_0x53c_sci.fit from the Pluto Cruise data set. Unfortunately, correcting the gradient also failed to yield any change in the stars' appearance.

Future Objectives

Capstone I has shown that using LEISA data for an EBL measurement is a much more difficult task than originally thought. In Capstone II, we hope to determine the feasibility of getting a good measurement of the EBL. If we conclude that EBL measurement is possible, then we will have to continue trying to mask stars and subtract the other contaminants outlined in Equation 1. However, our data will still be limited until the quaternion data is fixed. Even if we conclude that measuring the EBL is not possible, we will most definitely learn a lot about the instrument and what is needed in order to get a good measurement of the EBL. Also, there are still other objectives we could accomplish. This includes making a constraining measurement of the IPD and determine its implications in measuring the EBL. We could also attempt to use MVIC data to measure the EBL.

Timeline

Capstone II

- Filter data to find stars (4 weeks)
- Finalize Sensitivity estimate (2 weeks)
- Look for IPD signal and determine implications for EBL (5 weeks)
- Scientific Interpretation (2 weeks)
- Write paper and presentation (2 weeks)

Acknowledgments

I would like to thank Dr. Michael Zemcov for being my advisor in this project and for helping me through this process. I would also like to thank Teresa Symons for guiding me through questions I had on the material as well. I would like to thank Dr. Mishkatul Bhattacharya for his help in the capstone preparation class. Lastly, I would like to thank all the students and faculty in the School of Physics and Astronomy at RIT for all of their support.

---

* Rochester Institute of Technology, School of Physics and Astronomy, Faculty Advisor: Michael Zemcov

[1] Cooray, A. (2016). Extragalactic background light measurements and applications. Royal Society Open Science, 3(3), 150555. doi: 10.1098/rsos.150555

[2] Zemcov, Michael, and Teresa Symons. *The Optical Background with New Horizons*. pp. 1–15.

[3] Leinert, C. (1998). *The 1997 reference for diffuse sky brightness*. Astronomy and Astrophysics Supplementary Series, 1–99.

[4] Zemcov, M., Arcavi, I., ... Werner, M. (2018). *Astrophysics with New Horizons: Making the Most of a Generational Opportunity*. Publications of the Astronomical Society of the Pacific, 130(993), 115001.

[5] Dwek, E., & Hauser, M. G. (1998). The COBE Diffuse Infrared Background Experiment Search for the Cosmic Infrared Background. IV. Cosmological Implications. The Astrophysical Journal, 106–122. doi: 10.1086/306381

[6] Bernstein, R. A. (2007). *The Optical Extragalactic Background Light: Revisions and Further Comments*. The Astrophysical Journal, 666(2), 663–673. doi: 10.1086/519824

[7] Zemcov, M., Immel, P., Nguyen, C., Cooray, A., Lisse, C., & Poppe, A. (2016). *Measurement of the cosmic optical background using the long range reconnaissance imager on New Horizons*. Nature Communications, 1–7.

[8] Matsumoto, T., Matsuura, S., ... Noda, M. (2005). Infrared Telescope in Space Observations of the Near-Infrared Extragalactic Background Light. The Astrophysical Journal, 626(1), 31–43. doi: 10.1086/429383

[9] National Aeronautics and Space Agency.(2015). *New Horizons the First Mission to the Pluto System and Kuiper Belt*[Fact Sheet]. Retrieved from `https://www.nasa.gov/sites/default/files/atoms/files/nh-fact-sheet-2015_1.pdf`

[10] Reuter, D., Stern, A., ... Scherrer, J. (2008). *Ralph: A Visible/Infrared Imager for the New Horizons Pluto/Kuiper Belt Mission*. Space Science Review, 129–154.

[11] McCabe, George, and Allen Lunsford. "New Horizons SOC to Instrument Pipeline ICD." Retrieved from `pds-rings.seti.org/newhorizons/SOC_INST_ICD.PDF`.

[12] "NASA PDS: Small Bodies Node." SBN Mission Support: New Horizons, `pds-smallbodies.astro.umd.edu/data_sb/missions/newhorizons/index.shtml`.

[13] "NASA PDS: Small Bodies Node." SBN Mission Support: New Horizons Kuiper Belt Extended Mission, `pds-smallbodies.astro.umd.edu/data_sb/missions/nh-kem/index.shtml`.

[14] Beckett, Martin. "Rockwell PICNIC Array." Rockwell

PICNIC Array, people.ast.cam.ac.uk/~optics/tech/hawaii/picnic.htm.

[15] Souza, R. A., et al. "CMOS Image Sensor with FPN Reduction by Correlated Double Sampling in Current Mode." 2016 31st Symposium on Microelectronics Technology and Devices (SBMicro), 2016, doi:10.1109/sbmicro.2016.7731351.

[16] "Image Description Files." BIL, BIP, and BSQ Raster Files-Help — ArcGIS for Desktop,desktop.arcgis.com/en/arcmap/10.3/manage-data/raster-and-images/bil-bip-and-bsq-raster-files.htm.

[17] Gaia Collaboration, Gaia Data Release 2. Summary of the Contents and Survey ... ui.adsabs.harvard.edu/abs/2018A&A...616A...1G/abstract.

[18] "Cosmic Coordinates." Las Cumbres Observatory, lco.global/spacebook/sky/equatorial-coordinate-system/.

[19] Yang, Yaguang. "Spacecraft Attitude Determination." Spacecraft Modeling, Attitude Determination, and Control Quaternion-Based Approach, 2019, pp. 65–82., doi:10.1201/9780429446580-6.

[20] Bohlin, R. C., and R. L. Gilliland. "Hubble Space TelescopeAbsolute Spectrophotometry of Vega from the Far-Ultraviolet to the Infrared." The Astronomical Journal, vol. 127, no. 6, June 2004, pp. 3508–3515., doi:10.1086/420715.

[21] Bertin, Emmanuel. SExctractor v2.5 User's Manual. Institut d'Astrophysique & amp; Observatoire De Paris.